

On the Outage Performance of SWIPT Based Three-step Two-way DF Relay Networks

Yinghui Ye, Liqin Shi, Xiaoli Chu, *Senior Member, IEEE*, Hailin Zhang, *Member, IEEE*, and Guangyue Lu

Abstract—In this paper, we study the outage performance of simultaneous wireless information and power transfer (SWIPT) based three-step two-way decode-and-forward (DF) relay networks, where both power-splitting (PS) and “harvest-then-forward” are employed. In particular, we derive the expressions of terminal-to-terminal (T2T) and system outage probabilities based on a Gaussian-Chebyshev quadrature approximation, and obtain the T2T and system outage capacities. The effects of various system parameters, e.g., the static power allocation at the relay, symmetric PS, as well as asymmetric PS, on the outage performance of the investigated network are examined. It is shown that our derived expression for T2T outage capacity is more accurate than existing analytical results, and that the asymmetric PS achieves a higher system outage capacity than the symmetric one when the channels between the relay node and the terminal nodes have different statistic gains.

Index Terms—Outage performance, SWIPT based three-step two-way DF relay, power-splitting.

I. INTRODUCTION

SIMULTANEOUS wireless information and power transfer (SWIPT) has been recognized as a promising technology to alleviate the energy constraint in relay networks while maintaining reliable communications through a power-splitting (PS) or time-switching (TS) scheme [1], [2]. In a bidirectional transmission network, two-way relaying operates in two steps or three steps instead of four steps as required in one-way relaying, thus achieving a higher capacity [3]. In this regard, SWIPT based three-step (or two-step) two-way relay networks (TWRNs) are receiving increasing attention from the wireless industry and academia. Due to the limited space and our attention on SWIPT based three-step TWRNs, our work omits the literature review of SWIPT based two-step TWRNs, which can be referred to the art-of-the-state references [4]–[6].

As the low complexity of hardware is very important to energy-constrained networks, while the circuit of three-step TWRNs is simpler than that of two-step TWRNs, three-step TWRNs have attracted vast attention recently [3], [7]–[13]. The authors of [3] derived the terminal-to-terminal (T2T) outage probability, which considers the outage events at the terminal nodes independently, for three wireless power transfer schemes in TS based three-step amplify-and-forward (AF)

Manuscript received XXXX, revised XXXX. The research reported in this article was supported by the Natural Science Foundation of China (61801382), the Science and Technology Innovation Team of Shaanxi Province for Broadband Wireless and Application (2017KCT-30-02).

Yinghui Ye, Liqin Shi, and Hailin Zhang are with the Xidian University.

Xiaoli Chu is with the Department of Electronic and Electrical Engineering, The University of Sheffield, U.K. (e-mail: x.chu@sheffield.ac.uk).

Guangyue Lu is with the Xi’an University of Posts & Telecommunications, Xi’an, Shaanxi, P. R. China.

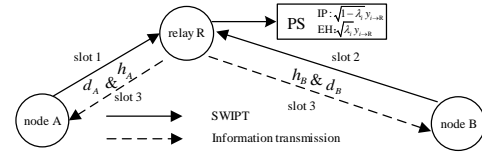


Fig. 1. System model of the three-step two-way DF relay network.

TWRNs. Considering three-step AF multiplicative TWRNs, the authors in [7] proposed a symmetric PS scheme¹ and investigated the T2T outage probability. To minimize the system outage probability, an optimal symmetric PS scheme and an optimal asymmetric scheme were developed in [8] and [9], respectively. Recently, three-step two-way relaying has been extended to DF relaying [10], where both upper and lower bounds of the T2T outage capacity were obtained for the symmetric PS scheme. The authors of [11] derived expressions of system outage probability for three-step TWRNs with TS(PS) SWIPT. To explore the advantages of both AF and DF relaying protocols, the authors studied the T2T performance of a SWIPT based three-step TWR with hybrid decode-amplify-forward (HDAF) [12]. The combination of SWIPT based three-step with other cognitive radio was reported in [13], aiming to analyze the system outage probability for the primary user and the secondary user.

Although these works mentioned above have laid a solid foundation for the understanding of SWIPT based three-step TWRNs, there are still large gaps needed to be filled. In particular, for a SWIPT based three-step DF TWRN, the existing theoretical expression of T2T outage capacity [10] is far from the simulation results. Besides, the authors in [11] and [13] focused on the analysis of system outage probability, while they ignored the channel reciprocity of terminal-relay links when deriving the expression of system outage probability. Accordingly, the system outage performance of SWIPT based three-step DF TWRNs is still far from being well understood. Motivated by the above observations, in this paper, we study the T2T and system outage probabilities of three-step DF TWRNs, where PS and “harvest-then-forward” are employed at the relay node, and derive expressions for both of them. Different from the T2T outage probability, the system outage probability evaluates the overall outage performance of both T2T links (i.e., the two one-way relay links) in the

¹In PS based three-step TWRNs, the relay is equipped with one power splitter and the PS ratios for both terminal-relay links may be unequal. If the PS ratios for two terminal-relay links are always equal, we refer to the PS scheme as the symmetric PS; otherwise, we refer to it as the asymmetric PS.

TWRNs, making the analysis and derivation much challenging than those of T2T outage performance. Based on the derived expressions, the impacts of various system parameters, such as the relay location and the energy conversion efficiency, on the system outage performance are analyzed. The performance comparison between symmetric and asymmetric PS schemes is also presented.

II. SYSTEM MODEL

We consider a DF TWRN, where two terminal nodes A and B exchange information with the aid of an energy-constrained relay node R based on a PS scheme, as shown in Fig. 1. The whole block time T has three transmission slots, where βT ($0 < \beta < 0.5$) is the time proportion for the relay to harvest energy and decode signal from one terminal node [10]. The ‘‘harvest-then-forward’’ scheme is adopted to encourage the relay to assist two terminal nodes. All nodes are equipped with a single antenna and operate in a half-duplex mode. We assume that there is no direct link between A and B. Note that our considered network can be applied to many energy-constrained wireless scenarios, e.g., the wireless sensor network in a toxic environments and the wireless body area network [11].

The channel model is given by $|h_i|^2 d_i^{-\alpha}$ ($i = A$ or B), where $h_i \sim \mathcal{CN}(0, \mu_i)$ is the i -R channel fading coefficient; d_i is the i -R distance; α is the path loss exponent. Thus the statistic channel gain of i -R link is given by $\mu_i d_i^{-\alpha}$. For analytical tractability, we further ignore the consumption of the transceiver circuitry at R [10].

At the first and the second time slots (each of the time slot is βT), nodes A and B transmit the normalized information signals x_A and x_B to the relay, respectively. The received signal at the relay R from terminal node i is $y_{i \rightarrow R} = h_i \sqrt{P_i d_i^{-\alpha}} x_i + n_{iR}$, where $n_{iR} \sim \mathcal{CN}(0, \sigma_{iR}^2)$ is the additive white Gaussian noise (AWGN) and P_i denotes the transmit power of terminal node i . Here, we assume that² $P_A = P_B = P_0$. Using the PS scheme, the received signal $y_{i \rightarrow R}$ is split to two parts: $\sqrt{\lambda_i} y_{i \rightarrow R}$ for energy harvesting (EH) and $\sqrt{1 - \lambda_i} y_{i \rightarrow R}$ for information processing. Thus, the total received energy from both terminal nodes and the received SNR from i to R are given by $E_{\text{total}} = P_0 \eta \beta T (\lambda_A |h_A|^2 d_A^{-\alpha} + \lambda_B |h_B|^2 d_B^{-\alpha})$ and $\gamma_{i \rightarrow R} = P_0 |h_i|^2 (1 - \lambda_i) d_i^{-\alpha} \sigma_{iR}^{-2}$, respectively, where η is the energy conversion efficiency and λ_i is the PS ratio of terminal node i . Note that λ_A may be different from λ_B in three-step relay networks, which makes it possible to more efficiently use of the received radio frequency (RF) signal at the relay.

Let \tilde{x}_i be the decoded signal for x_i . If both x_A and x_B are successfully decoded during the first two slots, then at the third time slot $(1 - 2\beta)T$ the relay R broadcasts the normalized signal $x_R = \theta_A x_A + \theta_B x_B$ to both terminal nodes using the harvested energy E_{total} , where $\theta_A^2 + \theta_B^2 = 1$ and θ_i^2 ($i = A, B$)

is a static³ power allocation ratio determining how the relay allocates the power for the decoded signals based on the statistic channel state information (CSI) (or statistic channel gain) of the i -R link. Thus, the received signal at terminal node i is given by $y_{R \rightarrow i} = h_i \sqrt{P_R d_i^{-\alpha}} x_R + n_{Ri} \stackrel{(a)}{=} h_i \sqrt{P_R d_i^{-\alpha}} \theta_i \tilde{x}_i + n_{Ri}$, where if $i = A, \bar{i} = B; i = B, \bar{i} = A; n_{Ri} \sim \mathcal{CN}(0, \sigma_{Ri}^2)$ is the AWGN; $P_R = \frac{E_{\text{total}}}{(1-2\beta)T}$ is the transmit power at R; step (a) holds under the assumption of perfect successive interference cancellation (SIC) [10]–[12]. This assumption is used here in order to obtain the upper bound of outage performance for our considered network.

Accordingly, the SNR of the $R \rightarrow i$ link is given by $\gamma_{R \rightarrow i} = \frac{\theta_i^2 \rho_0 \eta \beta}{(1-2\beta) d_i^\alpha} |h_i|^2 (\lambda_A |h_A|^2 d_A^{-\alpha} + \lambda_B |h_B|^2 d_B^{-\alpha})$, where $\rho_0 = \frac{P_0}{\sigma^2}$ and $\sigma_{AR}^2 = \sigma_{BR}^2 = \sigma_{RA}^2 = \sigma_{RB}^2 = \sigma^2$.

III. OUTAGE PROBABILITY ANALYSIS

A. Terminal-to-Terminal Outage Probability

Let $\mathbb{P}(\cdot)$ denote the probability and P_{out}^i be the outage probability of $i \rightarrow R \rightarrow i$ link. For a given target transmission rate U and the corresponding SNR threshold $\gamma_{\text{th}} = 2^U - 1$ [10], P_{out}^i is written as

$$P_{\text{out}}^i = 1 - P_1^i \quad (1)$$

where $P_1^i = \mathbb{P}(\gamma_{R \rightarrow i} \geq \gamma_{\text{th}}, \gamma_{\bar{i} \rightarrow R} \geq \gamma_{\text{th}})$.

Based on the expression of $\gamma_{R \rightarrow i}$ and $\gamma_{\bar{i} \rightarrow R}$, P_1^i can be rewritten as

$$\begin{aligned} P_1^i &= \mathbb{P}[|h_{\bar{i}}|^2 \geq \max(\Phi_{\bar{i}}, \Psi_{\bar{i}})] \\ &= \mathbb{P}[|h_{\bar{i}}|^2 \geq \Psi_{\bar{i}}, \Psi_{\bar{i}} \geq \Phi_{\bar{i}}] + \mathbb{P}[|h_{\bar{i}}|^2 \geq \Phi_{\bar{i}}, \Phi_{\bar{i}} > \Psi_{\bar{i}}] \quad (2) \end{aligned}$$

where $\Phi_{\bar{i}} = \frac{\gamma_{\text{th}} d_{\bar{i}}^\alpha}{\rho_0 (1 - \lambda_{\bar{i}})}$, $\Psi_{\bar{i}} = \frac{\gamma_{\text{th}} / X_i - \lambda_i |h_i|^4 d_i^{-\alpha}}{\lambda_{\bar{i}} |h_{\bar{i}}|^2} d_{\bar{i}}^\alpha$ and $X_i = \frac{\theta_i^2 \rho_0 \eta \beta}{(1-2\beta) d_i^\alpha}$.

When $\Psi_{\bar{i}} \geq \Phi_{\bar{i}}$, we have the following inequality

$$a_i |h_i|^4 + b_i |h_i|^2 - c_i \leq 0 \quad (3)$$

where $a_i = \lambda_i d_i^{-\alpha}$, $b_i = \frac{\gamma_{\text{th}} \lambda_i}{\rho_0 (1 - \lambda_i)}$ and $c_i = \gamma_{\text{th}} / X_i$.

Combining (3) with $|h_i|^2 \geq 0$, the range of $|h_i|^2$ is $0 \leq |h_i|^2 \leq \Omega_i$, where $\Omega_i = \frac{\sqrt{b_i^2 + 4a_i c_i} - b_i}{2a_i}$.

When $\Phi_{\bar{i}} > \Psi_{\bar{i}}$, we have $|h_i|^2 > \Omega_i$. Thus, P_1^i can be calculated as

$$\begin{aligned} P_1^i &= \mathbb{P}[|h_{\bar{i}}|^2 \geq \Phi_{\bar{i}}, |h_i|^2 > \Omega_i] + \mathbb{P}[|h_{\bar{i}}|^2 \geq \Psi_{\bar{i}}, 0 \leq |h_i|^2 \leq \Omega_i] \\ &= \exp\left(-\frac{\Phi_{\bar{i}}}{\mu_{\bar{i}}} - \frac{\Omega_i}{\mu_i}\right) + \frac{1}{\mu_i} \int_0^{\Omega_i} \exp\left(-\frac{\Psi_{\bar{i}}(y)}{\mu_{\bar{i}}} - \frac{y}{\mu_i}\right) dy \quad (4) \end{aligned}$$

where the second equality holds from $|h_i|^2 \sim \exp\left(\frac{1}{\mu_i}\right)$ for $i \in \{A, B\}$ and $y = |h_i|^2$.

Since it is difficult to find the closed-form expression for P_1^i due to the integral $\int_{s_1}^{s_2} \exp(z_1 x + \frac{z_2}{x}) dx$ for any value of

²The assumption will not cause any loss of generality to our analysis. This is because the average signal-to-noise-ratios (SNRs) of all channels are essential for the analysis of system outage performance, and the average SNRs depend on the transmit power at terminals and all the fading channels. Although $P_A = P_B$, the independent fading channels will have different values for their parameters, e.g., the distance of the terminal-relay link, making the average SNRs of all channels different.

³Note that the system capacity can be further improved if a dynamic power allocation ratio, which is adjusted based on the instantaneous CSI (or instantaneous channel gain) of terminal-relay links instead of statistic one, is adopted. This will be considered in our future work.

z_1 and $z_2 \neq 0$, we employ Gaussian-Chebyshev quadrature [2], [14] to obtain an approximation for P_1^i , as follows

$$P_1^i \approx \exp\left(-\frac{\Phi_i}{\mu_i} - \frac{\Omega_i}{\mu_i}\right) + \frac{\pi\Omega_i}{2N\mu_i} \sum_{n=1}^N \sqrt{1-\nu_n^2} \\ \times \exp\left(-\frac{\Psi_i(\chi_n^{(01)})}{\mu_i} - \frac{\chi_n^{(01)}}{\mu_i}\right) \quad (5)$$

where N is a parameter that determines the tradeoff between complexity and accuracy for the Gaussian-Chebyshev quadrature based approximation; $\nu_n = \cos \frac{2n-1}{2N}\pi$, and $\chi_n^{(01)} = \frac{\Omega_i}{2}\nu_n + \frac{\Phi_i}{2}$. Note that an acceptable accuracy can be achieved for a small value of N , which is verified in our simulations.

Submitting (5) into (1), we obtain the T2T outage probability for $\bar{i} \rightarrow R \rightarrow i$ link, P_{out}^i .

Thus, the outage capacity τ_{out}^i can be calculated as

$$\tau_{\text{out}}^i = \left(1 - P_{\text{out}}^i\right) U\beta T. \quad (6)$$

B. System Outage Probability

The system outage probability⁴ is defined as the probability that either the SNR of $\bar{i} \rightarrow i$ link is less than the SNR threshold γ_{th} . Thus, the system outage probability is written as

$$P_{\text{out}}^S = 1 - \mathbb{P}\left(\bigcup_{i=A,B} \gamma_{i \rightarrow R} \geq \gamma_{\text{th}}, \gamma_{R \rightarrow i} \geq \gamma_{\text{th}}\right) = 1 - P_1^S \quad (7)$$

where $P_1^S = 1 - \mathbb{P}(\bigcup_{i=A,B} |h_i|^2 \geq \max(\Phi_i, \Psi_i))$. Based on the expressions of Φ_i and Ψ_i defined in (2), P_1^S is rewritten as

$$P_1^S = P_{11}^S + P_{12}^S + P_{13}^S + P_{14}^S \quad (8)$$

where

$$P_{11}^S = \mathbb{P}(|h_A|^2 \geq \Psi_A, |h_B|^2 \geq \Phi_B, \Psi_A \geq \Phi_A, \Psi_B < \Phi_B) \\ P_{12}^S = \mathbb{P}(|h_B|^2 \geq \Psi_B, |h_A|^2 \geq \Phi_A, \Psi_A < \Phi_A, \Psi_B \geq \Phi_B) \\ P_{13}^S = \mathbb{P}(|h_B|^2 \geq \Phi_B, |h_A|^2 \geq \Phi_A, \Psi_A < \Phi_A, \Psi_B < \Phi_B) \\ P_{14}^S = \mathbb{P}(|h_B|^2 \geq \Psi_B, |h_A|^2 \geq \Psi_A, \Psi_A \geq \Phi_A, \Psi_B \geq \Phi_B).$$

1) P_{11}^S : If $\Psi_A \geq \Phi_A$ and $\Psi_B < \Phi_B$, we have

$$\begin{cases} a_B |h_B|^4 + b_A |h_B|^2 - c_B \leq 0 \\ a_A |h_A|^4 + b_B |h_A|^2 - c_A > 0 \end{cases} \quad (9)$$

Since $|h_A|^2 \geq 0$ and $|h_B|^2 \geq 0$, the solution to (9) is given by $0 \leq |h_B|^2 \leq \Omega_B$ and $|h_A|^2 > \Omega_A$, where $\Omega_i = \frac{\sqrt{b_i^2 + 4a_i c_i} - b_i}{2a_i}$, $i = A, B$. Then P_{11}^S can be computed as

$$P_{11}^S = \frac{1}{\mu_B} \int_{\Phi_B}^{\max(\Phi_B, \Omega_B)} \exp\left(-\frac{\phi_A(x)}{\mu_A} - \frac{x}{\mu_B}\right) dx \\ \approx \frac{\pi(\max(\Phi_B, \Omega_B) - \Phi_B)}{2N\mu_B} \sum_{n=1}^N \sqrt{1-\nu_n^2} \exp\left(-\frac{\phi_A(\chi_n^{(1)})}{\mu_A} - \frac{\chi_n^{(1)}}{\mu_B}\right) \quad (10)$$

where the approximation is obtained based on Gaussian-Chebyshev quadrature, $\phi_A(x) = \max(\Psi_A, \Omega_A)$, and $\chi_n^{(1)} = \frac{(\max(\Phi_B, \Omega_B) - \Phi_B)\nu_n + (\max(\Phi_B, \Omega_B) + \Phi_B)}{2}$.

⁴Note that, compared with traditional three-step TWRNs without SWIPT, the derivation of system outage probability in SWIPT based three-step TWRNs is more challenging since the transmit power of the relay depends on all the channel gains of terminal-relay links.

2) P_{12}^S : If $\Psi_A < \Phi_A$ and $\Psi_B \geq \Phi_B$, we have $0 \leq |h_A|^2 \leq \Omega_A$ and $|h_B|^2 > \Omega_B$. Similar to P_{11}^S , P_{12}^S can be calculated as

$$P_{12}^S \approx \frac{\pi(\max(\Phi_A, \Omega_A) - \Phi_A)}{2N\mu_A} \\ \times \sum_{n=1}^N \sqrt{1-\nu_n^2} \exp\left(-\frac{\phi_B(\chi_n^{(2)})}{\mu_B} - \frac{\chi_n^{(2)}}{\mu_A}\right) \quad (11)$$

where $\phi_B(x) = \max(\Psi_B, \Omega_B)$ with $|h_A|^2 = x$ and $\chi_n^{(2)} = \frac{(\max(\Phi_A, \Omega_A) - \Phi_A)\nu_n + (\max(\Phi_A, \Omega_A) + \Phi_A)}{2}$.

3) P_{13}^S : If $\Psi_A < \Phi_A$ and $\Psi_B < \Phi_B$, the ranges of $|h_B|^2$ and $|h_A|^2$ are determined by $|h_B|^2 > \Omega_B$ and $|h_A|^2 > \Omega_A$, respectively. Combining these ranges with $|h_B|^2 \geq \Phi_B$ and $|h_A|^2 \geq \Phi_A$, P_{13}^S can be computed as

$$P_{13}^S = \mathbb{P}(|h_B|^2 \geq \max(\Phi_B, \Omega_B), |h_A|^2 \geq \max(\Phi_A, \Omega_A)) \\ = \exp\left(-\frac{\max(\Phi_A, \Omega_A)}{\mu_A} - \frac{\max(\Phi_B, \Omega_B)}{\mu_B}\right). \quad (12)$$

4) P_{14}^S : If $\Psi_A \geq \Phi_A$ and $\Psi_B \geq \Phi_B$, both $0 \leq |h_B|^2 \leq \Omega_B$ and $0 \leq |h_A|^2 \leq \Omega_A$ should be satisfied. Then P_{14}^S can be denoted as

$$P_{14}^S = \mathbb{P}(\Psi_A \leq |h_A|^2 \leq \Omega_A, \Psi_B \leq |h_B|^2 \leq \Omega_B). \quad (13)$$

Note that $P_{14}^S = 0$ always holds for the case with $\Psi_A > \Omega_A$ or $\Psi_B > \Omega_B$. Since Ψ_A and Ψ_B are highly correlated, it is difficult to derive P_{14}^S . Let $|h_A|^2 = x$ and $|h_B|^2 = y$. We find that the integral region for calculating P_{14}^S is bounded by the following 4 lines: $y = \frac{\gamma_{\text{th}}/X_A - \lambda_A x^2 d_A^{-\alpha}}{\lambda_B x} d_B^\alpha$, $x = \frac{\gamma_{\text{th}}/X_B - \lambda_B y^2 d_B^{-\alpha}}{\lambda_A y} d_A^\alpha$, $x = \Omega_A$ and $y = \Omega_B$.

Let (x_1, y_Δ) denote the intersection of the lines $x = \Omega_A$ and $x = \frac{\gamma_{\text{th}}/X_B - \lambda_B y^2 d_B^{-\alpha}}{\lambda_A y} d_A^\alpha$. Then (x_1, y_Δ) is given by

$$x_1 = \Omega_A, y_\Delta = \frac{\sqrt{\lambda_A^2 x_1^2 + 4a_B c_B d_B^{2\alpha}} - \lambda_A x_1}{2a_B d_B^\alpha}. \quad (14)$$

Similarly, the intersection of the lines $y = \Omega_B$ and $y = \frac{\gamma_{\text{th}}/X_A - \lambda_A x^2 d_A^{-\alpha}}{\lambda_B x} d_B^\alpha$, (x_Δ, y_1) , is given by

$$x_\Delta = \frac{\sqrt{\lambda_B^2 y_1^2 + 4a_A c_A d_A^{2\alpha}} - \lambda_B y_1}{2a_A d_A^\alpha}, y_1 = \Omega_B. \quad (15)$$

The intersection of the lines $y = \Omega_B$ and $x = \frac{\gamma_{\text{th}}/X_B - \lambda_B y^2 d_B^{-\alpha}}{\lambda_A y} d_A^\alpha$ is denoted by (q_1, y_1) , where $q_1 = \frac{\gamma_{\text{th}}/X_B - \lambda_B y_1^2 d_B^{-\alpha}}{\lambda_A y_1} d_A^\alpha$. The intersection of the lines $x = \Omega_A$ and $y = \frac{\gamma_{\text{th}}/X_A - \lambda_A x^2 d_A^{-\alpha}}{\lambda_B x} d_B^\alpha$ is denoted by (x_1, q_2) , where $q_2 = \frac{\gamma_{\text{th}}/X_A - \lambda_A x_1^2 d_A^{-\alpha}}{\lambda_B x_1} d_B^\alpha$.

The intersection of the lines $x = \frac{\gamma_{\text{th}}/X_B - \lambda_B y^2 d_B^{-\alpha}}{\lambda_A y} d_A^\alpha$ and $y = \frac{\gamma_{\text{th}}/X_A - \lambda_A x^2 d_A^{-\alpha}}{\lambda_B x} d_B^\alpha$ is determined by

$$x = C_A/y - D_A y \text{ and } y = C_B/x - D_B x \quad (16)$$

where $C_i = \gamma_{\text{th}} d_i^\alpha / X_i \lambda_i$ and $D_i = \lambda_i d_i^\alpha / \lambda_i d_i^\alpha$. Substituting the $y = C_B/x - D_B x$ into $x = C_A/y - D_A y$, we have

$$-(C_A + C_B)x^2 + C_B^2 D_A = 0. \quad (17)$$

Since $x > 0$, the solution to (17) is given by $x_o = \sqrt{C_B^2 D_A / (C_A + C_B)}$, and the corresponding value of y is $y_o = C_B/x_o - D_B x_o$.

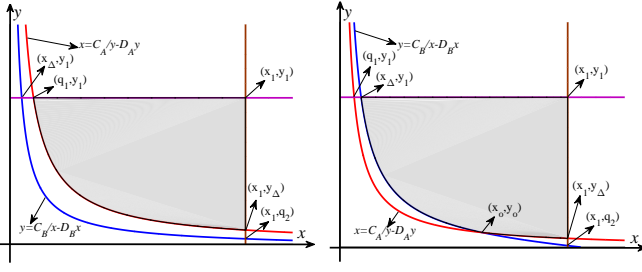


Fig. 2. The integral region for P_{14}^s in Case II with $y_{\Delta} \geq q_2$.

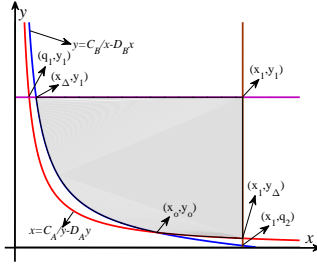


Fig. 3. The integral region for P_{14}^s in Case III with $y_{\Delta} \geq q_2$.

According to the values of intersections, the integral region for P_{14}^s can be divided into three cases.

Case I: If $\max(q_1, x_{\Delta}) \geq x_1$ or $\max(q_2, y_{\Delta}) \geq y_1$, the integral region is 0 and $P_{14}^s = 0$.

Case II: If $\max(q_1, x_{\Delta}) < x_1$, $\max(q_2, y_{\Delta}) < y_1$, and $x_o \leq \max(q_1, x_{\Delta})$ (or $x_o \geq x_1$), the integral region for P_{14}^s is bounded by the following three lines: $x = \Omega_A$, $y = \Omega_B$, and $y = C_B/x - D_B x$ (or $x = C_A/y - D_A y$).

When $y_{\Delta} \geq q_2$, the integral region for P_{14}^s is shown in Fig. 2. Accordingly, P_{14}^s is given by

$$\begin{aligned} P_{14}^s &= \mathbb{P}(\Psi_A \leq |h_A|^2 \leq x_1, y_{\Delta} \leq |h_B|^2 \leq y_1) \\ &= \frac{1}{\mu_B} \int_{y_{\Delta}}^{y_1} \exp\left(-\frac{C_A}{\mu_A y} + \left(\frac{D_A}{\mu_A} - \frac{1}{\mu_B}\right) y\right) dy - \varepsilon_A(x_1, y_{\Delta}, y_1) \\ &\approx \frac{\pi(y_1 - y_{\Delta})}{2N\mu_B} \sum_{n=1}^N \sqrt{1 - \nu_n^2} \exp\left(\kappa_A\left(\chi_n^{(3)}\right)\right) - \varepsilon_A(x_1, y_{\Delta}, y_1) \end{aligned} \quad (18)$$

where $\kappa_i\left(\chi_n^{(3)}\right) = -\frac{C_i}{\mu_i \chi_n^{(3)}} + \left(\frac{D_i}{\mu_i} - \frac{1}{\mu_i}\right) \chi_n^{(3)}$, $\chi_n^{(3)} = \frac{(y_1 - y_{\Delta})}{2} \nu_n + \frac{(y_1 + y_{\Delta})}{2}$, and $\varepsilon_i(x_1, y_{\Delta}, y_1) = \exp\left(-\frac{x_1}{\mu_i}\right) \left(\exp\left(-\frac{y_{\Delta}}{\mu_i}\right) - \exp\left(-\frac{y_1}{\mu_i}\right)\right)$.

Similarly, for the case with $y_{\Delta} < q_2$, P_{14}^s is given by

$$\begin{aligned} P_{14}^s &\approx \frac{\pi(x_1 - x_{\Delta})}{2N\mu_A} \sum_{n=1}^N \sqrt{1 - \nu_n^2} \exp\left(\kappa_B\left(\chi_n^{(4)}\right)\right) \\ &\quad - \varepsilon_B(y_1, x_{\Delta}, x_1) \end{aligned} \quad (19)$$

where $\chi_n^{(4)} = \frac{(x_1 - x_{\Delta})}{2} \nu_n + \frac{(x_1 + x_{\Delta})}{2}$.

Case III: If $\max(q_1, x_{\Delta}) < x_1$, $\max(q_2, y_{\Delta}) < y_1$, and $\max(q_1, x_{\Delta}) < x_o < x_1$, the integral region for P_{14}^s is bounded by four lines.

For the case with $y_{\Delta} \geq q_2$, the integral region for P_{14}^s is shown in Fig. 3 and P_{14}^s is given by

$$\begin{aligned} P_{14}^s &= \frac{1}{\mu_A} \int_{x_{\Delta}}^{x_o} \exp(\kappa_B(x)) dx + \frac{1}{\mu_B} \int_{y_{\Delta}}^{y_o} \exp(\kappa_A(y)) dy - \Lambda \\ &\approx \frac{\pi(x_o - x_{\Delta})}{2N\mu_A} \sum_{n=1}^N \sqrt{1 - \nu_n^2} \exp\left(\kappa_B\left(\chi_n^{(5)}\right)\right) \\ &\quad + \frac{\pi(y_o - y_{\Delta})}{2N\mu_B} \sum_{n=1}^N \sqrt{1 - \nu_n^2} \exp\left(\kappa_A\left(\chi_n^{(6)}\right)\right) - \Lambda \end{aligned} \quad (20)$$

where $\Lambda = \varepsilon_B(y_1, x_{\Delta}, x_o) - \varepsilon_A(x_1, y_{\Delta}, y_o) + \varphi(x_o, x_1, y_o, y_1)$, $\varphi(x_o, x_1, y_o, y_1) = \left(\exp\left(-\frac{x_o}{\mu_A}\right) - \exp\left(-\frac{x_1}{\mu_A}\right)\right) \left(\exp\left(-\frac{y_o}{\mu_B}\right) - \exp\left(-\frac{y_1}{\mu_B}\right)\right)$, $\chi_n^{(5)} = \frac{(x_o - x_{\Delta})}{2} \nu_n + \frac{(x_o + x_{\Delta})}{2}$ and $\chi_n^{(6)} = \frac{(y_o - y_{\Delta})}{2} \nu_n + \frac{(y_o + y_{\Delta})}{2}$.

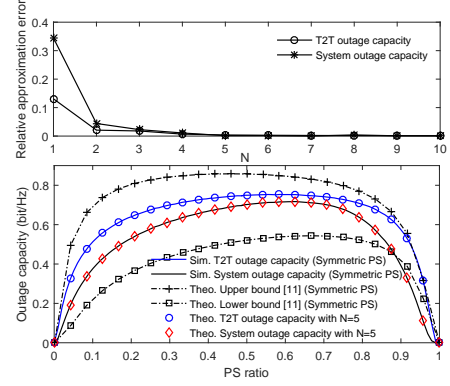


Fig. 4. The accuracy of our derived results.

For the case with $y_{\Delta} < q_2$, P_{14}^s is given by

$$\begin{aligned} P_{14}^s &= \frac{1}{\mu_A} \int_{x_o}^{x_1} \exp(\kappa_B(x)) dx + \frac{1}{\mu_B} \int_{y_o}^{y_1} \exp(\kappa_A(y)) dy \\ &\quad - \varepsilon_B(y_o, x_o, x_1) - \varepsilon_A(x_1, y_o, y_1) \\ &\approx \frac{\pi(x_1 - x_o)}{2N\mu_A} \sum_{n=1}^N \sqrt{1 - \nu_n^2} \exp\left(\kappa_B\left(\chi_n^{(7)}\right)\right) - \varepsilon_B(y_o, x_o, x_1) \\ &\quad + \frac{\pi(y_1 - y_o)}{2N\mu_B} \sum_{n=1}^N \sqrt{1 - \nu_n^2} \exp\left(\kappa_A\left(\chi_n^{(8)}\right)\right) - \varepsilon_A(x_1, y_o, y_1) \end{aligned} \quad (21)$$

where $\chi_n^{(7)} = \frac{(x_1 - x_o)}{2} \nu_n + \frac{(x_o + x_1)}{2}$ and $\chi_n^{(8)} = \frac{(y_1 - y_o)}{2} \nu_n + \frac{(y_o + y_1)}{2}$. Substituting (10), (11), (12) and (18) (or (19), or (20), or (21), or 0) into (8) and (7), P_{out}^s is determined.

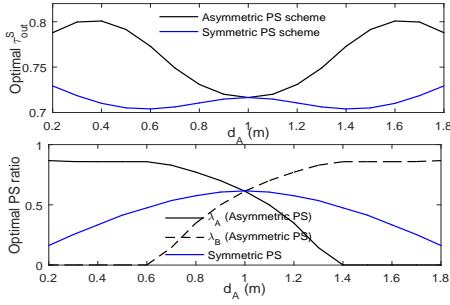
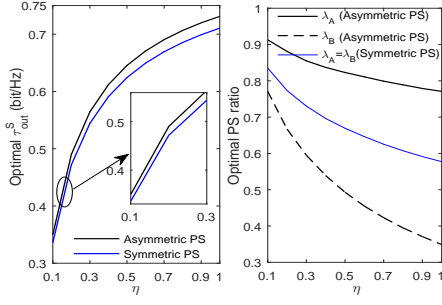
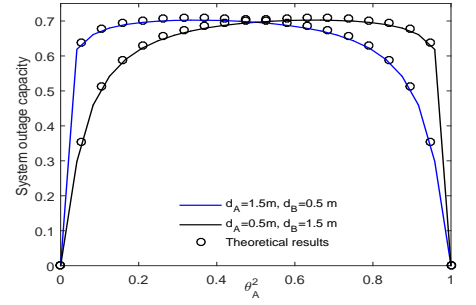
The system outage capacity τ_{out}^s is given as

$$\tau_{\text{out}}^s = (1 - P_{\text{out}}^s) U \beta T. \quad (22)$$

Remark 1. The derived results can serve the following purposes. The first purpose is to obtain an accurate outage capacity with a small N instead of the computer simulations. The second purpose is to observe some insights regarding the design of the PS ratios and the static power allocation ratio from the curves obtained by the derived results. In our considered network, the PS ratios and the static power allocation ratio are designed based on the statistic channel gains instead of instantaneous channel gains, it is practical to obtain the insights offline regarding the design of PS ratios and the static power allocation ratio and such approach has also adopted in many works, e.g., [6]. A concrete example is Fig. 5 of the revised manuscript, where the optimal system outage capacity and PS ratios for two PS schemes are obtained by maximizing the derived system outage capacity expression as in problem (23). It can be observed that the optimal λ_i decreases with the increase of the statistic channel gain of i -R link.

$$\begin{aligned} \max_{\lambda_A, \lambda_B} \quad & \tau_{\text{out}}^s \\ \text{s.t.} \quad & 0 \leq \lambda_A, \lambda_B \leq 1 \end{aligned} \quad (23)$$

Lastly, we can obtain the diversity gain of the considered network, shown in the next subsection.


 Fig. 5. Optimal τ_{out}^S and PS ratio versus d_A .

 Fig. 6. Optimal τ_{out}^S and PS ratio versus η .

 Fig. 7. System outage capacity versus θ_A^2 .

C. Diversity Analysis

The diversity gain is written as

$$d = - \lim_{\rho_0 \rightarrow \infty} \frac{\log(1 - P_{11}^s - P_{12}^s - P_{13}^s - P_{14}^s)}{\log(\rho_0)}. \quad (24)$$

It is not hard to verify that $\lim_{\rho_0 \rightarrow \infty} P_{11}^s = \lim_{\rho_0 \rightarrow \infty} P_{12}^s = \lim_{\rho_0 \rightarrow \infty} P_{14}^s = 0$ and $\lim_{\rho_0 \rightarrow \infty} P_{13}^s = 1$. Thus, the diversity gain can be rewritten as

$$d = - \lim_{\rho_0 \rightarrow \infty} \frac{\log(1 - P_{13}^s)}{\log(\rho_0)}. \quad (25)$$

Now let us compare Ω_i and Φ_i . When the transmit SNR approaches infinite, we have

$$\lim_{\rho_0 \rightarrow \infty} \frac{\Omega_i}{\Phi_i} = \infty. \quad (26)$$

Combining (26) and the fact that Ω_i and Φ_i decrease with ρ_0 , we have

$$\lim_{\rho_0 \rightarrow \infty} \max(\Omega_i, \Phi_i) = \lim_{\rho_0 \rightarrow \infty} \Phi_i. \quad (27)$$

Thus, the diversity gain can be calculated as

$$d = - \lim_{\rho_0 \rightarrow \infty} \frac{\log\left(1 - \exp\left(-\frac{1}{\rho_0}\right)\right)}{\log(\rho_0)} \stackrel{x=\frac{1}{\rho_0}}{=} \lim_{x \rightarrow 0} \frac{x}{1 - \exp(-x)} = 1. \quad (28)$$

IV. SIMULATIONS

Here, simulation results are provided to verify the derived expressions of (6) and (22). We adopt the same system parameter settings as in [10] for fair comparison between (6) and the existing T2T outage capacity [10]. Fig. 4 plots the relative approximate error versus N , as well as the outage capacity as a function of the PS ratio by assuming that $\lambda_A = \lambda_B$ as in [10]. For the upper part of Fig. 4, we assume that $\lambda_A = \lambda_B = 0.2$. It can be seen that the relative approximation error [15] decreases with N , and that our approximated results are sufficient to provide level of accuracy within very few items (e.g. $N \geq 5$). For the lower part of Fig. 4, the upper and lower bounds of the T2T outage probability from [10] are also provided. The theoretical T2T outage capacity and system outage capacity with $N = 5$ are computed based on (6) and (22), respectively. It can be observed that the derived theoretical results match perfectly with the simulation results,

which validates the correctness of the theoretical results. In particular, the derived theoretical results are accurate enough with $N = 5$ no matter what the PS ratio is, which verifies our approximation again. Besides, the derived T2T outage capacity is more accurate than that in [10], which is one of the contributions of this paper. Another observation is that the achievable capacity increases first and then decreases with PS ratio, i.e., there only exists an optimal pair of symmetric PS ratio to maximize the achievable capacity.

Fig. 5 plots the optimal system outage capacity and PS ratio as a function of the distance of A – R link d_A with two PS schemes, respectively. The two PS schemes for comparison are the symmetric PS scheme and asymmetric PS scheme where both λ_A and λ_B are adjustable and the existing symmetric PS scheme with $\lambda_A = \lambda_B$ as in [10]. The optimal system outage capacity and PS ratios for two PS schemes are obtained by maximizing the derived system outage capacity expression, as in (23). It is difficult to derive closed-form solutions for the problem (23) by using conventional solution methods. But we can use genetic algorithm-Based Algorithm to solve (23) (Please see Section 6 of [11] as an example). For convenience, we adopt the two-dimensional search algorithm to obtain the optimal PS ratios in Fig. 5 of the revised manuscript. It is assumed that the relay is located on the straight line between the both terminal nodes, i.e., $d_A + d_B = 2$. Note that here $d_A \neq d_B$ results in the unequal statistic channel gains between the relay and the terminal nodes. One can see that the asymmetric PS scheme provides a higher capacity compared with the symmetric PS scheme when $d_A \neq d_B$, while achieving the same capacity at $d_A = d_B$. The reasons are as follows. The asymmetric PS scheme provides more flexibility than the symmetric PS scheme and the optimal PS ratios are determined by the statistic channel gains. If statistic channel gains are unequal, the asymmetric PS scheme makes two different optimal PS ratios and achieves a higher capacity; otherwise, the optimal PS ratios of the asymmetric PS scheme satisfy $\lambda_A = \lambda_B$ and the PS ratio is equal to that of the symmetric PS scheme. One also can see that, in the asymmetric PS scheme, the relay harvests more (or less) energy with a larger (or smaller) PS ratio from the terminal node with a better (or worse) statistic channel to the relay, which achieves a trade-off between EH and information processing for the two terminal nodes.

Fig. 6 describes the relations of the optimal system outage

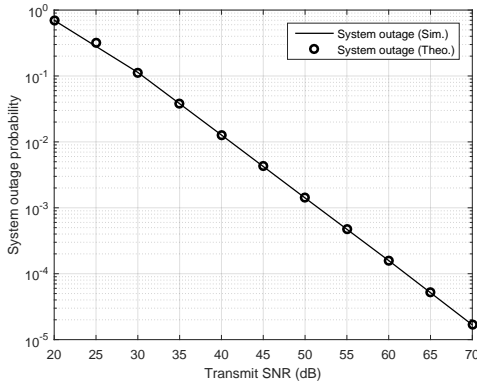


Fig. 8. System outage probability against transmit SNR.

capacity and PS ratios against the η , respectively. Here we set d_A and d_B as 0.8 and 1.2, respectively. It can be seen that, with the increasing of η , the optimal system outage capacity increases, while the optimal PS ratios decrease. The reasons are as follows. Based on (7) and (22), it is not hard to that the maximum system outage capacity is to maximize $\min \left\{ \bigcup_{i=A,B} \gamma_{i \rightarrow R} \geq \gamma_{th}, \gamma_{R \rightarrow i} \geq \gamma_{th} \right\}$. If η increases, $\gamma_{R \rightarrow A}$ and $\gamma_{R \rightarrow B}$ will increase. In order to maximize the system outage capacity, $\gamma_{A \rightarrow R}$ and $\gamma_{B \rightarrow R}$ should be improved, which can be realized by decreasing the optimal PS ratios. It can also be seen that the asymmetric PS scheme outperforms the symmetric one especially for a higher η .

In Fig. 7, we plot system capacity versus static power allocation ratio θ_A^2 with different relay locations for $\lambda_A = \lambda_B = 0.5$. It can be observed that the theoretical results match simulation results well, demonstrating the accuracy of our derived expression. Besides, there exists an optimal θ_A^2 and the optimal θ_A^2 is highly dependent on the relay location. To maximize the system capacity, the relay should assign less power to x_B when the relay is close to terminal A; otherwise, the relay should allocate more power to x_A . Finally, Fig. 8 verifies the diversity analysis.

V. CONCLUSIONS

In this paper, we have studied the outage performance of three-step DF TWRNs with PS SWIPT. The expressions for T2T and system outage probabilities (and capacities) have been derived and verified by computer simulations. Some insights regarding the asymmetric PS scheme have been obtained. First, the optimal PS ratios are sensitive to the relay location and the energy conversion efficiency. In particular, the optimal λ_i decreases with the increase of the statistic channel gain of i -R link. With the increase of the energy conversion efficiency, the optimal ratios, λ_A and λ_B , show a downward trend. Second, the asymmetric PS scheme outperforms the symmetric one for the unequal statistic channel gains between the relay node and the terminal nodes. Third, the selection of power allocation ratio is highly related with the relay location.

This work can be extended by relaxing the assumption of perfect SIC, making our considered network close to practical scenario.

REFERENCES

- [1] W. Guo, S. Zhou, Y. Chen *et al.*, "Simultaneous information and energy flow for IoT relay systems with crowd harvesting," *IEEE Commun. Mag.*, vol. 54, no. 11, pp. 143–149, November 2016.
- [2] Y. Ye, Y. Li, D. Wang, F. Zhou, R. Q. Hu, and H. Zhang, "Optimal transmission schemes for DF relaying networks using SWIPT," *IEEE Trans. Veh. Technol.*, vol. 67, no. 8, pp. 7062–7072, 2018.
- [3] Y. Liu, L. Wang, M. ElKashlan, T. Q. Duong, and A. Nallanathan, "Two-way relaying networks with wireless power transfer: Policies design and throughput analysis," in *Proc. GLOBECOM*, Dec 2014, pp. 4030–4035.
- [4] S. Modem and S. Prakriya, "Optimization of two-way relaying networks with battery-assisted EH relays," *IEEE Trans. Commun.*, pp. 1–1, 2018.
- [5] S. Zhong, H. Huang, and R. Li, "Outage probability of power splitting SWIPT two-way relay networks in nakagami-m fading," *EURASIP J. Wireless Commun. Network.*, vol. 2018, no. 1, p. 11, 2018.
- [6] S. Modem and S. Prakriya, "Performance of analog network coding based two-way EH relay with beamforming," *IEEE Trans. Commun.*, vol. 65, no. 4, pp. 1518–1535, April 2017.
- [7] S. T. Shah, K. W. Choi, S. F. Hasan, and M. Y. Chung, "Energy harvesting and information processing in two-way multiplicative relay networks," *Electron. Lett.*, vol. 52, no. 9, pp. 751–753, 2016.
- [8] Z. Wang, Y. Li, Y. Ye, and H. Zhang, "Dynamic power splitting for three-step two-way multiplicative AF relay networks," in *Proc. IEEE VTC-Fall*, Sept 2017, pp. 1–5.
- [9] Y. Ye, Y. Li, Z. Wang, X. Chu, and H. Zhang, "Dynamic asymmetric power splitting scheme for SWIPT based two-way multiplicative AF relaying," *IEEE Signal Proc. Lett.*, vol. 25, no. 7, pp. 1014–1018, 2018.
- [10] N. T. P. Van, S. F. Hasan, X. Gui, S. Mukhopadhyay, and H. Tran, "Three-step two-way decode and forward relay with energy harvesting," *IEEE Commun. Lett.*, vol. 21, no. 4, pp. 857–860, April 2017.
- [11] R. Jiang, K. Xiong, Y. Zhang, and Z. Zhong, "Outage analysis and optimization of SWIPT in network-coded two-way relay networks," *Mobile Inf. Syst.*, vol. 2017, Feb. 2017, Art. no. 2516035.
- [12] D. S. Gurjar, U. Singh, and P. K. Upadhyay, "Energy harvesting in hybrid two-way relaying with direct link under nakagami-m fading," in *Proc. IEEE WCNC*, April 2018, pp. 1–6.
- [13] A. Mukherjee, T. Acharya, and M. R. A. Khandaker, "Outage analysis for SWIPT-enabled two-way cognitive cooperative communications," *IEEE Trans. Veh. Technol.*, vol. 67, no. 9, pp. 9032–9036, Sept 2018.
- [14] Y. Liu *et al.*, "Cooperative non-orthogonal multiple access with simultaneous wireless information and power transfer," *IEEE J. Sel. Areas Commun.*, vol. 34, no. 4, pp. 938–953, April 2016.
- [15] C. Zhang *et al.*, "A unified approach for calculating the outage performance of two-way AF relaying over fading channels," *IEEE Trans. Veh. Technol.*, vol. 64, no. 3, pp. 1218–1229, March 2015.